RESEARCH ARTICLE

Simulation of tissue heating by magnetic fluid hyperthermia

Seyed Nasrollah Tabatabaei[1]*; Sylvain Martel[2]

[1]Department of Medical Nanotechnology, Tehran University of Medical Sciences, Tehran, Iran

[2]NanoRobotics Laboratory, Department of Computer and Software Engineering, Institute of Biomedical Engineering, Polytechnique Montréal, Montréal, Canada

ARTICLE INFO

Article History:
Received 19 November 2017
Accepted 25 December 2017
Published 31 December 2017

Keywords:
Magnetic drug targeting
Drug delivery
Hyperthermia
Magnetotactic bacteria

ABSTRACT

Objective(s): Magnetic fluid hyperthermia is a technique in which thermal energy is generated by magnetic nanoparticles (MNPs) that are excited by an alternating magnetic field (AC field). During hyperthermia, in-vivo monitoring of elevation of temperature relies on invasive insertion of conventional thermometers, or employment of thermo-sensitive cameras that lack high precision. The objective of this manuscript is to provide a mathematical approach to better estimate elevation of temperature and its profile after hyperthermia of MNPs inside an AC field. **Methods:** To this end, we first show that temperature profile due to hyperthermia of iron oxide MNPs at 10, 25, and 50 mg/ml are concentration dependent. Then by using best-fit polynomial equations, we show that the temperature profile for any given concentration of the same iron oxide MNPs can be traced to close approximation. Thermodynamic heat transfer equations were then used to graph the distribution of temperature in a tissue with a known heat capacity and conductivity parameters.

Results: The resulting MatLab software simulation provides the thermal profile of a hypothetical tumor placed adjacent to a muscle tissue.

Conclusions: In conclusion, the proposed mathematical approach can closely estimate the temperature profile of magnetic fluid hyperthermia.

How to cite this article
Tabatabaei S N , Martel S, Simulation of tissue heating by magnetic fluid hyperthermia, Nanomed Res J, 2017; 2(4):260-266.
DOI: 10.22034/nmrj.2017.04.007

INTRODUCTION

Hyperthermia is an elevation of body temperature beyond its normal range. In medicine, hyperthermia is used as a rehabilitation method and therefore it is often referred to as thermal (heat) therapy or thermotherapy. Mild hyperthermia can reduce arthritis pain, relieve muscle spasms, reduce inflammation, and increase blood flow to provide nutritious needs to injured tissue [1]. On the other hand, hyperthermia can provide cytotoxicity effects that may lead to cellular apoptosis [2]. The cell death rate varies depending on the sustained temperature and the duration of hyperthermia. In oncology, hyperthermia refers to the heating of organs or tissues in various ways, to temperatures between 40°C and 45°C, at which point it causes moderate and reversible cellular inactivation. This heat can lead to preferential death of malignant cells by enhancing cell sensitivity and vulnerability to more established forms of cancer therapy such as radiation and chemotherapy (thermal chemosensitization, thermal radiosensitization) [3]. Studies show that hyperthermia of tumor cells can lead to a synergistic effect in anti-cancer techniques such as chemotherapy [4]. More specifically, hyperthermia can be seen as a complementary therapy that yields maximum benefit from chemotherapeutic agents, while minimizing their applied dosage to the

* Corresponding Author Email: *ntabatabaei@sina.tums.ac.ir*

physiological system and thus reducing the toxic side effects that harm healthy cells. In addition, tumors often lack a sophisticated vascular structure and a natural cooling system [5]. Consequently, tumors are more prone to high temperatures.

Clinically, hyperthermia can be created artificially by means of drugs [6] or medical devices such as high intensity focused ultrasound [7], microwave radiation [8], radiofrequency antennas [9], laser irradiation [10], magnetic fluid hyperthermia [11], and sometimes, a combination of two or more of the mentioned techniques [12]. Among different applications of hyperthermia, actuation for drug release [13], drug delivery across the blood-brain barrier [14] and the blood-retinal barrier [15], as well as neural stimulations [16] have been the focus of recent research. In this manuscript, we focus on a mathematical technique to simulate temperature elevation due to magnetic fluid hyperthermia.

Generation of heat in magnetic fluid hyperthermia is due to excitation of magnetic nanoparticles (MNPs) from exposure to an alternating magnetic field (AC field). Under the influence of the field, MNPs undergo relaxation mechanisms (Neel and Brownian) and release their absorbed energy from the field in the form of heat to their surroundings [11]. In addition, MNPs have enormous potential in biomedical applications such as imaging, medical diagnosis, and treatment [17]. In contrast to other forms, hyperthermia of MNPs provides advanced control on thermal distribution and can be highly localized.

An experimental setup for hyperthermia of MNPs consists of an induction coil connected to an amplifier, with which the AC field is generated, a sample inside the coil that contains MNPs, and a thermometer (thermocouples, thermal imaging cameras such as IR, or fiber optic temperature sensors, etc.) to measure and record elevation of temperature. While temperature measurements in this experimental setup are conventional, empirical temperature monitoring in a biological tissue is challenging. Insertion of any temperature probe inside the patient is invasive, IR cameras are not accurate, and the heterogeneous nature of most tissues (heat conductivity) and small scale of MNPs make it nearly impossible for any temperature probe to record temperature elevation during hyperthermia. In this manuscript, we first show that for any given concentration of MNPs under hyperthermia, the resulting elevation of temperature and its profile is closely correlated to other concentrations of the same MNPs. We then use mathematical equations to approximate temperature behaviour of the MNPs inside a biological entity during hyperthermia.

MATERIALS AND METHODS

Iron Oxide MNPs

In this investigation, nanoparticles were purchased from micromod (Rostock-Warnemuende, Germany) and their magnetic properties as well as core diameter were verified by a vibrating sample magnetometer (VSM: EV5, Magnetics) and transmission electron microscopy (TEM: Jeol JEM-2100 operated at 200 kV). According to TEM analysis (Figure 1a), the core diameters of the particles vary in two narrow size distributions peaking at 10 nm and 12 nm (Figure 1b). The VSM results reported a magnetization saturation MS value near 43 emu/g for these nanoparticles. This is almost half of the values found in the literature for bulk magnetite (Figure 1c). The atomic absorption spectrometry (AAS: Thermo Scientific S Series) confirmed that the nanoparticles were uniformly suspended in an aqueous solution and contained 50% dextran as their coating. Last but not least, X-ray diffraction analysis confirmed the crystal structure of the MNPs to be iron oxide (Figure 1d).

Experimental Setup

For this investigation, a 1.5 kW induction heating machine (Norax Canada Inc, Quebec, Canada), was used to provide a magnetic field near 80 kA/m (~1000 Oe) at a frequency of 150 kHz inside the coil. Prior to the experiment, the particles were divided into three concentration groups of 10 mg/ml, 25 mg/ml and 50 mg/ml of suspension fluid by means of distillation. Each sample was then placed in custom made isolation Styrofoam (see Figure 2) fitted for the inside of a 13 mm diameter, 8 turn copper tube induction coil. Styrofoam minimizes the effect of possible external temperature fluctuations from the coil or variation of room temperature by thermally insulating the sample. Temperature changes were monitored and recorded at every 15 seconds for a period of 900 seconds (15 minutes) by two thermocouples (T-Type, Omega HH506R). A thermocouple measured the temperature of the sample and the

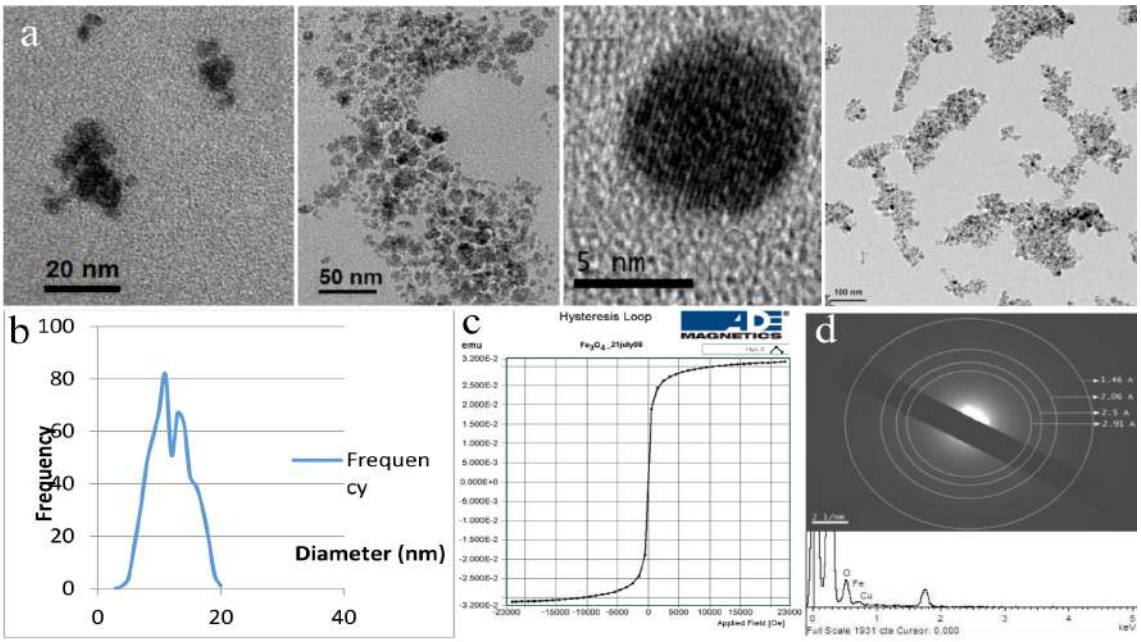

Fig. 1. a) MNPs purchased from micromod observed by TEM, b) Size distribution of MNPs, c) Hysteresis curve of MNPs by vibrating sample magnetometer (VSM: EV5, Magnetics), d) Illustrates the crystal diffraction patterns corresponding to magnetite (Fe3O4) as the chemical composition of the particles.

other measured the temperature of the Styrofoam as shown in Figure 2.

Prior to any test, a sample containing 1ml of deionized water was placed inside the coil to measure the effect of the AC field on the suspension medium, the thermocouples, the sample container, and the Styrofoam. Such effect was measured to be negligible for this experiment. The tests were carried out at least three times for each sample and the results were averaged.

Data analysis

Once the temperature data were acquired, MatLab (MathWorks) was used to theoretically analyse and plot the results.

RESULTS AND DISCUSSION

Under the condition where AC field parameters were constant, temperature rose more rapidly as concentration of MNPs were increased from 10 mg/ml to 25 mg/ml (Figure 3). This was not far from our expectation. MNPs can be seen as miniaturized heat sources that activate when placed inside the AC field. By increasing the concentration of MNPs, we have basically increased the number of available heat sources in the sample thereby we see higher

Fig 2. Experimental setup where MNPs in different concentrations were placed in an isolation foam that was fitted for the inside of the cylindrical coil attached to the hyperthermia machine. Thermocouple probes measured the temperature of the MNPs and the isolation foam.

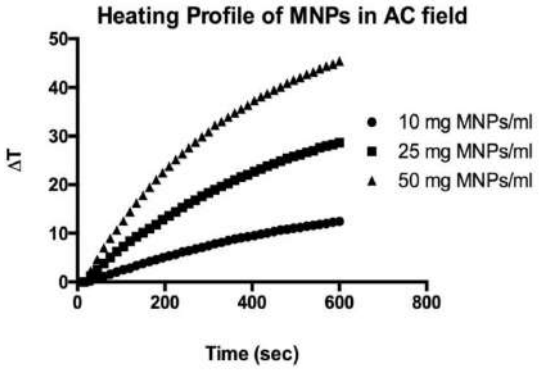

Fig 3. Hyperthermia of MNPs at 3 concentrations of 10, 25, and 50 mg/ml and the resulting temperature profile

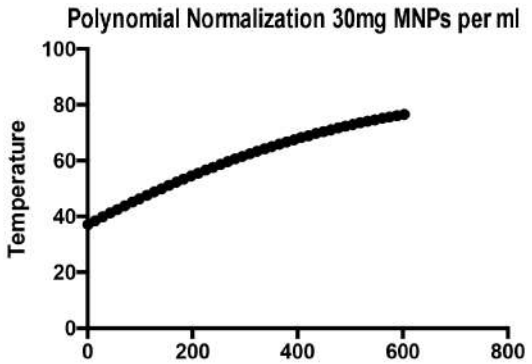

Fig 4. Simulation of temperature as a function of time for 30 mg magnetite per ml fluid (30 mg magnetite per ml due to 50% dextran coating)

temperatures.

Plotted curves in Figure 3 suggest that, for all samples, initial temperature rise follows a sub-linear trend, then after some time the thermal exchange between the sample and the surrounding area reaches near equilibrium. It is fair to speculate that eventually ΔT becomes zero. In hyperthermia, Specific Absorption Rate (SAR) is a measurement of the energy (in this case magnetic energy) absorbed per unit mass of the material (W/g). SAR is proportional to the time rate of change of the temperature of the magnetic material and given by the following Equation 1 [18]:

$$SAR = \frac{c\,V_s}{m}\frac{dT}{dt} \qquad (1)$$

$$\Delta T = \mathrm{SAR}\frac{\mathrm{C}\,R^2}{3\lambda} \qquad (2)$$

where c is the specific heat capacity of the sample (4185 J/l/K for water), m is the mass of the magnetic particles, V_s is the total volume and dT/dt expressed in °K/s is the temperature increment which is experimentally derived from the linear regression of the initial data points seen on in Figure 3. Table 1 tabulates calculated SAR values estimated from plots shown in Figure 3 (graphical SAR) using the above equation. As seen in table below, dT/dt is steeper for samples with higher mass (g/ml). SAR is a ratio, therefore, it is independent of the concentration of the MNPs and should be equal for all samples. The difference in SAR that is seen in the table however, could be explained by possible experimental errors due to unintentional small changes in the AC field or frequency as well as slight changes in the room temperature.

Using the graphical SAR values, ΔT (at the initial linear section of the curve – t=200 s) can also be mathematically approximated using Equation (2) where C is the concentration of the MNPs (mass of the particles per tissue volume) and λ represents the heat conductivity of a 1 ml volume (0.146 W/K/m) with a radius R (4.5 mm radius of the vial containing the sample).

Theoretical and experimental ΔT follow the same incrementing trend and the values are in close agreement. In order to estimate final values, temperature profiles can be plotted as a function of time to fit second order polynomial equations. These equations are shown in Table 3.

In fact, the linear trend seen above may help

Table 1. SAR graphical measurement based on Equation 1

Concentration: mg (Fe_3O_4 MNP +50% Coating) per ml Fluid	*50*	*25*	*10*
mass: mg magnetite per ml Fluid	25	12.5	5
$\frac{dT}{dt}$ *(°C/s)*	0.124	0.071	0.028
SAR (W/g)	20.758	23.791	23.921

Table 2. Theoretical and experimental estimations for ΔT based on Equation 2

Concentration (coating + MNP) mg/ml	Experimental ΔT (at t=200 sec)	Theoretical ΔT Using Eq. (2)
10	5.4	5.53
25	13.6	13.75
50	24.8	23.99

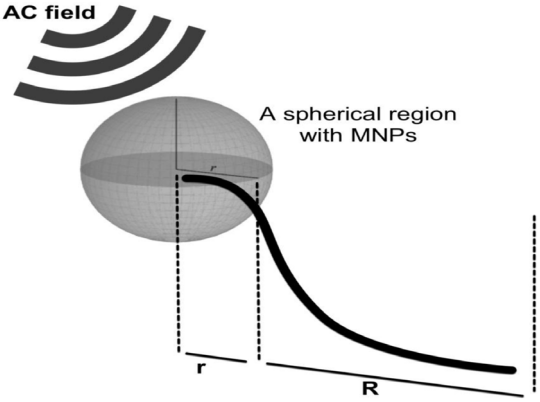

Fig 5. Temperature vs. Distance

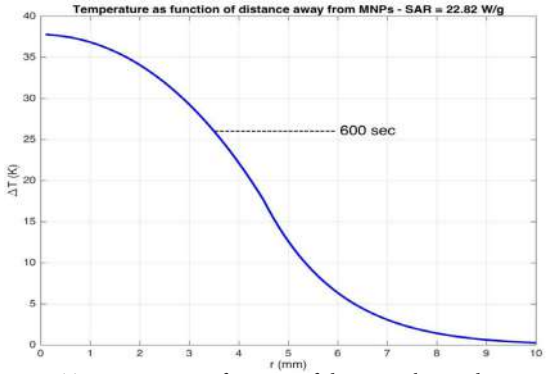

Fig 6. Temperature as a function of distance, thermodynamic equations predict the temperature drop as we get away from the center of the hyperthermic action.

formation of a systematic relationship between concentration of MNPs and the final temperature for any given time interval. For instance, at 37°C, under the same AC field parameters, the second order polynomial equation for 1ml sample of the same MNPs with a concentration of 30 mg per ml (15 mg magnetite per ml) would have approximately a x and x^2 ratio of 1:3 and therefore can be approximated to be $y=-5.7 \times 10^{-5}x^2+ 0.1x + 37$. Figure 4 predicts that in 600 seconds, the approximated temperature reaches 76.6 °C.

Once the above estimations were obtained, thermodynamic equations can be used to estimate the distribution of heat into the surrounding tissue. Considering the average SAR value of 22.82 W/g (obtained from Table 1), we can estimate the behaviour of the MNPs in a biological entity. For practical purposes, Figure 5 demonstrates this concept, in which r represents the distance from the center of a spherical volume to a point at infinity. Temperature at the surface of the spherical volume is $T_{Initial}$ and reaches minimum temperature T_{Final} (steady state) at a distance r=∞. It is assumed that the temperature inside the spherical volume is constant.

The following time-dependent thermodynamic heat transfer equations [19] were used in MatLab to sketch a graphical simulation of ΔT as a function of distance for five arbitrary time values in Figure 6:

$$\Delta T_1(r,t) = \frac{PR^2}{6\lambda_1}\left[1+\frac{q_\lambda}{2}\left(1-\frac{r^2}{R^2}\right)+\frac{6}{\pi}q_\lambda^{\frac{3}{2}}q^{\frac{1}{2}}\frac{R}{r}\int_0^\infty f(z;r,t)g_1(z;r)dz\right] \quad (3)$$

for $0 \le r < R$

$$\Delta T_2(r,t) = \frac{PR^3}{3\lambda_2 r}\left[1+\frac{6}{\pi}q_\lambda\int_0^\infty f(z;r,t)g_2(z;r)\frac{dz}{z}\right] \quad (4)$$

for $r > R$

With the abbreviations:

$$q_\lambda = \frac{\lambda_2}{\lambda_1}$$

$$q = \frac{\rho_2 c_2}{\rho_1 c_1}$$

$$s(z) = (q_\lambda - 1)\sin z + z\cos z$$

$$f(z;r,t) = z^{-2}\exp\left(-\frac{\lambda_1 t z^2}{\rho_1 c_1 R^2}\right) \times \frac{z\cos z - \sin z}{[s(z)]^2 + q_\lambda q(z\sin z)^2}$$

$$g_1(z;r) = \sin\left(\frac{rz}{R}\right)$$

$$g_2(z;r) = s(z)\sin[k(z;r)] + (q_\lambda q)^{\frac{1}{2}} z\sin z\ \cos[k(z;r)]$$

$$k(z;r) = \left(\frac{q}{q_\lambda}\right)^{\frac{1}{2}} z\left(\frac{r}{R}-1\right)$$

where P is the SAR multiplied by density of particles at the region (3.18×10^5 g/m^3), λ_1 (0.778 W/K/m) and λ_2 (0.642 W/K/m) represent values of heat conductivity for a hypothetical medium

Table 3. Second order polynomial best-fit for normalized thermal profile of hyperthermia of MNPs

MNPs Concentration	Second Order Polynomial	x^2 a [10 mg/ml]ca: a [MNPs]	x b [10 mg/ml]: b [MNPs]
10	$y = -1.9 \times 10^{-5} x^2 + 0.033\, x$	1:1	1:1
25	$y = -4.9 \times 10^{-5} x^2 + 0.078\, x$	1:2.57	1:2.36
50	$y = -10 \times 10^{-5} x^2 + 0.14\, x$	1:4.90	1:4.24

1 in a tumor ("for" 0≤r<R) and another adjacent hypothetical medium 2 in the muscle tissue ("for " r>R), respectively, c_1 (2.54 J/g/K) and c_2 (3.72 J/g/K) are heat capacity coefficients of medium 1 and 2, and ρ_1 (1.66 x 106 g/m3) and ρ_2 (1 x 106 g/m3) are mass densities for the medium 1 and 2, respectively. The parameter z is to help integrate from 0 to infinity and does not have a physical meaning. The graph in Figure 6 is plotted using a numerical integration technique. To estimate thermal effect in various tissues, values of λ,c,ρ for different biological tissues can be taken from literature [20]. The curve in Figure 6 represents the thermal dissipation with respect to distance from the center of spherical volume (r = 4.5 mm) for 600 seconds. As expected, temperature drops rapidly a few millimetres away from the surface of R. This means that in a hyperthermia application, unnecessary heat can be kept away from healthy surrounding tissue. Last but not least, the initial ΔT in Figure 6 is in accordance with our ΔT findings presented in Fiugre 4.

CONCLUSIONS

In oncology, hyperthermia refers to the heating of organs or tissues in various ways, to temperatures between 40°C and 45°C, at which point it causes moderate and reversible cellular inactivation. This heat can lead to preferential death of malignant cells. The multi-functionality nature of MNPs and their controllable physical parameters are the motives behind ever growing interest in hyperthermia of MNPs among scientists around the world. However, measurement of elevation of temperature in a biological entity is very challenging. In this manuscript, thermal behaviour of several concentrations of MNPs under hyperthermia of AC field are recorded. Then, quadratic polynomial equations best-fitting the observed behaviour were traced. The resulting information helped trace the thermal behaviour of any other concentration of the same MNPs. Then the distribution of thermal energy in a hypothetical tissue were calculated using thermodynamic heat transfer equations. Last but not least, MatLab software was used to draw thermal profile of a tumor placed adjacent to a muscle tissue.

CONFLICTS OF INTEREST

The authors declare that there are no conflicts of interest regarding the publication of this manuscript.

REFERENCES

1. Rosenberg H, Pollock N, Schiemann A, Bulger T, Stowell K. Malignant hyperthermia: a review. Orphanet journal of rare diseases, 2015;10 (1):93.
2. Hou C-H, Lin F-L, Hou S-M, Liu J-F. Hyperthermia induces apoptosis through endoplasmic reticulum and reactive oxygen species in human osteosarcoma cells. International journal of molecular sciences, 2014;15 (10):17380-17395.
3. Roesch M, Mueller-Huebenthal B. The role of hyperthermia in treating pancreatic tumors. Indian journal of surgical oncology, 2015;6 (1):75-81.
4. Hegyi G, Szigeti GP, Szász A. Hyperthermia versus oncothermia: cellular effects in complementary cancer therapy. Evidence-Based Complementary and Alternative Medicine, 2013;2013.
5. Rieger H, Welter M. Integrative models of vascular remodeling during tumor growth. Wiley Interdisciplinary Reviews: Systems Biology and Medicine, 2015;7 (3):113-129.
6. Walter E, Carraretto M. Drug-induced hyperthermia in critical care. Journal of the Intensive Care Society, 2015;16 (4):306-311.
7. Copelan A, Hartman J, Chehab M, Venkatesan AM. High-intensity focused ultrasound: current status for image-guided therapy. Seminars in interventional radiology. Vol 32: Thieme Medical Publishers; 2015:398.
8. Peeken JC, Vaupel P, Combs SE. integrating Hyperthermia into Modern Radiation Oncology: what evidence is Necessary? Frontiers in oncology, 2017;7:132.
9. Ho JC, Nguyen L, Law JJ, Ware MJ, Keshishian V, Lara N, Nguyen T, Curley SA, Corr SJ. Non-Invasive Radiofrequency Field Treatment to Produce Hepatic Hyperthermia: Efficacy and Safety in Swine. IEEE journal of translational engineering in health and medicine, 2017;5:1-9.
10. Schena E, Saccomandi P, Fong Y. Laser ablation for cancer: past, present and future. Journal of functional biomaterials, 2017;8 (2):19.
11. Ng EYK, Kumar SD. Physical mechanism and modeling of heat generation and transfer in magnetic fluid hyperthermia through Néelian and Brownian relaxation: a review. Biomedical engineering online, 2017;16 (1):36.
12. McWilliams BT, Wang H, Binns VJ, Curto S, Bossmann SH, Prakash P. Experimental Investigation of Magnetic Nanoparticle-Enhanced Microwave Hyperthermia. Journal of functional biomaterials, 2017;8 (3):21.
13. Tabatabaei SN, Lapointe J, Martel S. Shrinkable hydrogel-based magnetic microrobots for interventions in the vascular network. Advanced Robotics, 2011;25 (8):1049-1067.

14.Tabatabaei SN, Girouard H, Carret A-S, Martel S. Remote control of the permeability of the blood–brain barrier by magnetic heating of nanoparticles: a proof of concept for brain drug delivery. Journal of Controlled Release, 2015;206:49-57.

15.Tabatabaei SN, Tabatabaei MS, Girouard H, Martel S. Hyperthermia of magnetic nanoparticles allows passage of sodium fluorescein and Evans blue dye across the blood–retinal barrier. International Journal of Hyperthermia, 2016;32 (6):657-665.

16.Tay A, Di Carlo D. Remote Neural Stimulation Using Magnetic Nanoparticles. Current medicinal chemistry, 2017;24 (5):537-548.

17.Gobbo OL, Sjaastad K, Radomski MW, Volkov Y, Prina-Mello A. Magnetic nanoparticles in cancer theranostics. Theranostics, 2015;5 (11):1249.

18.Lévy M, Wilhelm C, Siaugue J-M, Horner O, Bacri J-C, Gazeau F. Magnetically induced hyperthermia: size-dependent heating power of γ-Fe2O3 nanoparticles. Journal of Physics: Condensed Matter, 2008;20 (20):204133.

19.Andrä W, d'Ambly C, Hergt R, Hilger I, Kaiser W. Temperature distribution as function of time around a small spherical heat source of local magnetic hyperthermia. Journal of Magnetism and Magnetic Materials, 1999;194 (1-3):197-203.

20.Barnes FS, Greenebaum B. Biological and medical aspects of electromagnetic fields: CRC press; 2006.